BIOINFORMATICS ORIGINAL PAPER

Vol. 29 no. 10 2013, pages 1299–1307
doi:10.1093/bioinformatics/btt140

Systems biology

Advance Access publication April 23, 2013

A unifying kinetic framework for modeling oxidoreductase-catalyzed reactions

Ivan Chang[1,2] and Pierre Baldi[2,3,*]

[1]Department of Biomedical Engineering, [2]Institute for Genomics and Bioinformatics and [3]Department of Computer Science, University of California, Irvine, CA 92697, USA

Associate Editor: Mario Albrecht

ABSTRACT

Motivation: Oxidoreductases are a fundamental class of enzymes responsible for the catalysis of oxidation–reduction reactions, crucial in most bioenergetic metabolic pathways. From their common root in the ancient prebiotic environment, oxidoreductases have evolved into diverse and elaborate protein structures with specific kinetic properties and mechanisms adapted to their individual functional roles and environmental conditions. While accurate kinetic modeling of oxidoreductases is thus important, current models suffer from limitations to the steady-state domain, lack empirical validation or are too specialized to a single system or set of conditions.

Results: To address these limitations, we introduce a novel unifying modeling framework for kinetic descriptions of oxidoreductases. The framework is based on a set of seven elementary reactions that (i) form the basis for 69 pairs of enzyme state transitions for encoding various specific microscopic intra-enzyme reaction networks (micro-models), and (ii) lead to various specific macroscopic steady-state kinetic equations (macro-models) via thermodynamic assumptions. Thus, a synergistic bridge between the micro and macro kinetics can be achieved, enabling us to extract unitary rate constants, simulate reaction variance and validate the micro-models using steady-state empirical data. To help facilitate the application of this framework, we make available RedoxMech: a Mathematica™ software package that automates the generation and customization of micro-models.

Availability: The Mathematica™ source code for RedoxMech, the documentation and the experimental datasets are all available from: http://www.igb.uci.edu/tools/sb/metabolic-modeling.

Contact: pfbaldi@ics.uci.edu

Supplementary information: Supplementary data are available at *Bioinformatics* online.

Received on August 7, 2012; revised on March 18, 2013; accepted on March 21, 2013

1 INTRODUCTION

Oxidoreductase, the first enzyme class in the Enzyme Commission Nomenclature (EC 1.x.x.x, henceforth referred to as EC 1), consists of enzymes responsible for the catalytic transfer of electrons from an electron donor molecule to an electron acceptor molecule. The universal presence of oxidoreductases in the energy-producing pathways of bacteria, archaea and eukaryotes suggests that these proteins arose earlier during the process of biogenesis, and are thus essential for life (Berry, 2002). In the EC 1, oxidoreductases are classified according to the types of donor and acceptor molecules in the particular oxidation–reduction (redox) reaction that they participate in (http://www.brenda-enzymes.org), although the kinetics and regulatory behaviors of enzymes in the same classification may differ significantly across different organisms, or even across different tissues in the same organism (Benard *et al*., 2006; Vinogradov, 2008).

To understand the functional role an oxidoreductase has within a pathway, and to characterize its differences from other oxidoreductases, it is necessary to be able to predict accurately its dynamics over a range of conditions. However, a full realization of the dynamics of an oxidoreductase is currently hindered by (i) the lack of detailed structural and mechanistic information on most of the oxidoreductases, e.g. complex I–NADH dehydrogenase (Brandt, 2006), (ii) the technological limitations in obtaining the specific elementary kinetic rate constants and (iii) the computational limitations associated with molecular dynamics and other physical simulations over large spatial and temporal scales (Klepeis *et al*., 2009). To bypass these limitations, simplified models are used, which typically follow either the macroscopic modeling approach of deducing a steady-state velocity equation to represent the rate of the reaction, or the microscopic kinetic approach of defining a system of intra-enzyme processes to represent the detailed kinetic mechanisms of the enzyme.

A macroscopic steady-state velocity equation is a mathematical relationship between reactant concentrations and empirically derived kinetic parameters that provides a steady-state deterministic solution to the flux of the reactants through the enzyme. The relationship can be a simple hyperbolic function, such as the Michaelis–Menten kinetic equation, or a more complex function derived from a macroscopic approximation of many elementary reactions at steady state (Chen *et al*., 2010). Kinetic models based on steady-state velocity equations are widely used and published because steady-state kinetic parameters are relatively easy to acquire via available measurement techniques, and the steady-state 'snap-shots' of their dynamics can readily be compared (Sin *et al*., 2009). For example, in our previous work (Chang *et al*., 2011), a two-substrate and two-product (Bi Bi) steady-state velocity equation termed the chemiosmotic rate law was derived for the chemiosmotic oxidoreductase complexes in the mitochondria, and corresponding enzyme assay protocols were developed and implemented to estimate the values of the kinetic parameters in the rate law and enable comparison across various cell lines. However, steady-state velocity equations are based on many approximations and steady-state assumptions that severely limit

*To whom correspondence should be addressed.

their range of applicability. Furthermore, although deterministic solutions can satisfactorily describe the average behavior of the enzyme over many ensembles that are consistent with *in vitro* experimental conditions, they might not accurately capture *in vivo* conditions within a cell or a cell's organelle, where the significantly lower volume and thus fewer copies of the enzyme and its reactants and stochastic fluctuations may become important (Rao and Arkin, 2003). Thus, many kinetic features of the enzyme could be over-estimated (e.g. the parameter values), under-estimated (e.g. stochastic variability of the velocity) or altogether lost (e.g. transient phase of the reaction).

Microscopic kinetic models avoid the various steady-state approximations by explicitly accounting for the intra-enzyme reactions and solving the corresponding system of ordinary differential equations (ODEs; Selivanov *et al.*, 2009, 2011). Kinetic models based on intra-enzyme reactions not only can produce a more complete deterministic description of the enzyme kinetics, but can also be used in conjunction with Monte-Carlo methods such as Gillespie's stochastic simulation algorithm (SSA) to produce stochastic time series, which can capture the intrinsic variability of the catalyzed reaction (Ransac *et al.*, 2008, 2010). However, in contrast to the velocity equations, the rate constants of the intra-enzyme reactions are not only harder to obtain experimentally (Mulquiney and Kuchel, 2003), but also less useful in comparison between models owing to the lack of standards between the various possible enzyme mechanisms.

Here we present a novel framework for modeling oxidoreductase-catalyzed reactions that uses a synergistic combination of both macroscopic and microscopic kinetic model descriptions of the reaction system (henceforth referred to as macro-model and micro-model, respectively) to obviate the aforementioned modeling limitations. At the core of this unifying framework is a basis of seven elementary reactions. This basis can be used to express various mechanisms of oxidoreductase by (i) defining the specific micro-model out of the 69 pairs of feasible enzyme microstate transitions spanned from the seven elementary reactions, and (ii) inferring the corresponding specific macro-model through temporal separation and non-equilibrium thermodynamic assumptions. We show that, by sharing the same abstraction, the unitary rate constants of the micro-model can be estimated from the experimentally determinable steady-state parameters of the macro-model to produce the same steady-state output. In contrast, the intrinsic stochasticity of the enzyme captured by the micro-model simulations can be superimposed onto the macro-model time series. Additionally, we show how well-known mechanisms can be encoded by the micro-model, how these mechanisms differ in their transient and steady-state domains and how they can be combined to simulate a cascade or a supercomplex. The application of this framework is facilitated by a Mathematica™ software package, RedoxMech, which generates customizable micro-models through simple xCellerator-like arrow notations for chemical reactions.

2 METHODS

2.1 EC 1 reaction decomposition

2.1.1 General processes In general, an EC 1 enzyme binds to donor and acceptor electron carriers (e-carriers) and facilitates the flow of electrons between them and through the enzyme–substrate complex by a series of internal redox steps with an overall chemical reaction of

$$v_{dr}D^{red} + v_{ao}A^{ox} \rightleftharpoons v_{do}D^{ox} + v_{ar}A^{red}$$

where D^{ox} and D^{red} are the oxidized and reduced species of the donor e-carrier reactant (D), A^{ox} and A^{red} are the oxidized and reduced species of the acceptor e-carrier reactant (A), and v_{dr}, v_{do}, v_{ao} and v_{ar} represent their stoichiometric reaction coefficients, respectively. In this work, we focus on the derivation of the framework for the most common Bi Bi reaction where the stoichiometric reaction coefficients are all set to the value of 1, but note that other coefficient variations (and thus molecularity reactions such as Bi Uni, Bi Ter, Ter Ter and higher) can readily be extended from the methods demonstrated in this framework.

While the exact sequences of the internal redox reactions are usually unknown and highly variable across different EC 1 enzymes, a universal mode of operation is that electrons are transferred to and from an oxidoreductase complex after the necessary reactant e-carriers are bound and situated within distance for electron tunneling between the external e-carrier and a close-by internal redox center (Chang *et al.*, 2011). Thus, the catalytic operation of an EC 1 enzyme can be decomposed into three spatially distinct processes (Fig. 1):

(1) Binding/unbinding of donor and acceptor e-carriers to/from the complex.

(2) Electron transfer between the e-carriers and the boundary redox centers of the complex.

(3) Central 'black-box' catalytic electron transfer between the redox centers.

This separation of fundamental processes enables elementary reactions of the overall chemical reaction to be defined below.

2.1.2 Elementary reactions A set of seven microscopic reactions can be obtained through the defined boundaries of the three fundamental processes (Fig. 1). Of the seven, four are associated with the

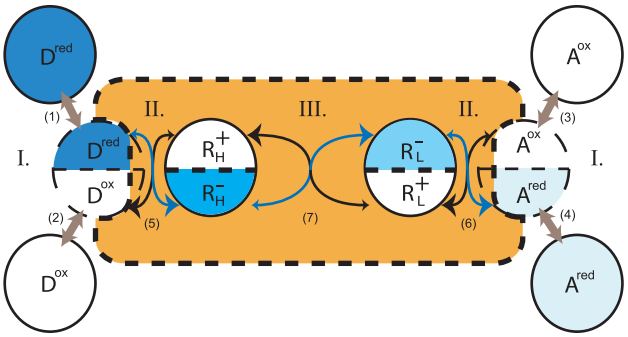

Fig. 1. An EC 1 reaction. The Bi Bi oxidoreductase reaction is shown here as the elementary interactions between a representative EC 1 enzyme, and its donor and acceptor e-carrier reactants, D and A, respectively. The blue lines represent the path of the electron transfer, whereas the blue shades represent the relative redox potential (the darker, the higher). The introduction of the two internal redox centers, R_H and R_L, allows one to spatially separate the overall reaction into three general processes: I. reactants binding/unbinding; II. e-transfers between bound reactants and internal redox centers; and III. central catalytic e-transfer between internal redox centers. Within the three processes, one can further enumerate seven elementary reaction pairs shown here with number indexes, where 1–4 represent elementary binding reaction pairs (grey double arrows), and 5–7 represent three elementary redox reaction pairs (blue/black arrows)

reactant-binding/unbinding processes, whereas three are associated with the electron transfer processes. At the microscopic level, the binding/unbinding processes of the e-carrier reactants associated with an EC 1 enzyme can be considered independently as four individual elementary reactions, which are expressed (with their forward and reverse unitary rate constants) as

$$D^{red} + Enz \rightleftharpoons D^{red}Enz \qquad (kf_{D^{red}}, kr_{D^{red}}) \tag{1}$$

$$D^{ox} + Enz \rightleftharpoons D^{ox}Enz \qquad (kf_{D^{ox}}, kr_{D^{ox}}) \tag{2}$$

$$A^{ox} + Enz \rightleftharpoons A^{ox}Enz \qquad (kf_{A^{ox}}, kr_{A^{ox}}) \tag{3}$$

$$A^{red} + Enz \rightleftharpoons A^{red}Enz \qquad (kf_{A^{red}}, kr_{A^{red}}) \tag{4}$$

For the internal electron transfer processes of the complex, a 'high potential' redox center R_H and a 'low potential' redox center R_L are introduced to represent the internal redox centers at the boundaries next to the reactant-binding sites (Fig. 1) such that the overall chemical reaction can be partitioned into three subreactions:

$$\nu_{do}D^{red} + R_H^+ \rightleftharpoons \nu_{do}D^{ox} + R_H^- \qquad (kf_{D,R_H}, kr_{D,R_H}) \tag{5}$$

$$R_H^- + R_L^+ \rightleftharpoons R_H^+ + R_L^- \qquad (kf_{cat}, kr_{cat}) \tag{6}$$

$$R_L^- + \nu_{ao}A^{ox} \rightleftharpoons R_L^+ + \nu_{ar}A^{red} \qquad (kf_{R_L,A}, kr_{R_L,A}) \tag{7}$$

where Equation (5) describes the elementary electron transfer reaction between the donor e-carrier and the R_H redox center, Equation (6) describes the lumped catalytic electron transfer reaction and Equation (7) describes the elementary electron transfer reaction between the R_L redox center and the acceptor e-carrier. In the absence of additional knowledge of the catalytic process encapsulated in the lumped reaction, Equation (6) can be considered as an approximated elementary reaction for simplicity. Equations (1–7) form the core kinetic description of the framework from which both microscopic and macroscopic models can be derived, as detailed in the following subsections.

2.2 EC 1 micro-model

The elementary reactions can be explicitly and individually modeled to give the microscopic behavior of the reaction system. The different ways that the seven elementary reactions can be interconnected to enable the flow of electrons between the donor and acceptor e-carriers give rise to a variety of feasible kinetic mechanisms belonging to EC 1. Thus, to represent all kinetic mechanisms under this framework, we encode the intra-enzyme reaction network of a prototypical EC 1 enzyme in terms of all possible enzyme–substrate redox states (henceforth referred to as the microstates) and the transitions between them. The transition probabilities are the unitary rate constants of the corresponding elementary reactions. In a general-to-specific approach, this 'complete' intra-enzyme reaction network can, in turn, be used as a generating model from which all other intra-enzyme reaction networks representing specific EC 1 mechanisms can be derived as reduced subsets by pruning certain transitions. The enumeration of all possible microstates and transitions within this framework proceeds as follows.

2.2.1 Microstates Because each EC 1 enzyme has two boundary redox centers (R_H, R_L) that can be either reduced or oxidized for 2^2 states, and two binding sites (donor, acceptor) that can each be in one of three states (empty, bound reduced e-carrier, bound oxidized e-carrier) for 3^2 states, there is a grand total of $2^2 \times 3^2$ or 36 microstates for an EC 1 enzyme complex. The 36 microstates are categorized by their molecularity (4 unimolecular, 16 bimolecular and 16 trimolecular) and enumerated in Table 1.

2.2.2 State Transitions From the categories of microstates, one can form 16 uni-to-bimolecular reversible transitions and 32 bi-to-trimolecular reversible transitions for a total of 48 transition pairs representing the binding reactions for an EC 1 complex, each pair consisting of one forward and one reverse transition between two different states. These binding transitions can be sorted by the molecularity of the products (bi for bimolecular and ter for trimolecular) and the binding sequence of the reactant e-carriers (donor first, acceptor first, donor second, acceptor second). Thus, the unitary rate constants for the binding transitions may be classified as follows: bi-donor first (D1), bi-acceptor first (A1), ter-donor second (D2) and ter-acceptor second (A2). In addition to the binding transitions, there are 21 feasible electron transfer transitions pairs, which can be organized by their molecularity (uni, bi and ter) and the reaction type {donor boundary [Equation (5)], catalytic [Equation (6)] and acceptor boundary [Equation (7)]}. The unitary rate constants for the electron transfer reactions are classified as follows: uni-catalytic transfer (UT), bi-donor boundary (BD), bi-acceptor boundary (BA), bi-catalytic transfer (BT), ter-donor boundary (TD), ter-acceptor boundary (TA) and ter-catalytic transfer (TT). Table 2 provides a short categorized summary of all 69 possible state transitions, while detailed listings of elementary reaction equations for each organizational group can be found in Appendix B of Supplementary Materials. From this set of feasible state transitions, specific intra-enzyme reaction network can be defined through the unitary rate constants, dictating which transitions are more probable than others. Several prominent cases, out of a spectrum of possible mechanisms, are shown in Section 3.

2.3 EC 1 macro-model

The seven elementary reactions can also be combined into a steady-state velocity equation to represent a specific macro-model, provided that the macroscopic relationships between the elementary reactions are defined. Although an exact equation can be derived from the intra-enzyme reaction network of a micro-model through the use of the King–Altman method (Cornish-Bowden, 1977), the resulting equation ends up containing a complex arrangement of the unitary rate constants instead of the experimentally measurable kinetic parameters (see Appendix C of

Table 1. Enzyme states of the micro-model (microstates)

Unimolecular	Bimolecular				Trimolecular			
Epp	Dre◇Epp	Dox◇Epp	Epp◇Aox	Epp◇Are	Dre◇Epp◇Aox	Dre◇Epp◇Are	Dox◇Epp◇Aox	Dox◇Epp◇Are
Epn	Dre◇Epn	Dox◇Epn	Epn◇Aox	Epn◇Are	Dre◇Epn◇Aox	Dre◇Epn◇Are	Dox◇Epn◇Aox	Dox◇Epn◇Are
Enp	Dre◇Enp	Dox◇Enp	Enp◇Aox	Enp◇Are	Dre◇Enp◇Aox	Dre◇Enp◇Are	Dox◇Enp◇Aox	Dox◇Enp◇Are
Enn	Dre◇Enn	Dox◇Enn	Enn◇Aox	Enn◇Are	Dre◇Enn◇Aox	Dre◇Enn◇Are	Dox◇Enn◇Aox	Dox◇Enn◇Are

Note: Reactants and enzyme states are displayed in Mathematica-friendly format, with Dre = D^{red}, Dox = D^{ox}, Aox = A^{ox}, Are = A^{red}, Epp = Enz[R_H^+, R_L^+], Epn = Enz[R_H^+, R_L^-], Enp = Enz[R_H^-, R_L^+], Enn = Enz[R_H^-, R_L^-], ◇ = bond.

Table 2. Classification of all microstate transitions within the micro-model of EC 1

Reaction group	Equation number	Unitary rates	Transition pairs
Bi-donor first (D1)	1, 2	kf_{D1}, kr_{D1}	8
Bi-acceptor first (A1)	3, 4	kf_{A1}, kr_{A1}	8
Ter-donor second (D2)	1, 2	kf_{D2}, kr_{D2}	16
Ter-acceptor second (A2)	3, 4	kf_{A2}, kr_{A2}	16
Ter-donor boundary (TD)	5	kf_{TD}, kr_{TD}	4
Ter-catalytic transfer (TT)	6	kf_{TT}, kr_{TT}	4
Ter-acceptor boundary (TA)	7	kf_{TA}, kr_{TA}	4
Bi-donor boundary (BD)	5	kf_{BD}, kr_{BD}	2
Bi-catalytic transfer (BT)	6	kf_{BT}, kr_{BT}	4
Bi-acceptor boundary (BA)	7	kf_{BA}, kr_{BA}	2
Uni-catalytic transfer (UT)	6	kf_{UT}, kr_{UT}	1
Total			69

Supplementary Materials). Therefore, additional approximate but well-posed assumptions are necessary to deduce the relationship between the corresponding micro and macro-models in the context of measurable parameters. Our previous work on the chemiosmotic rate law (Chang *et al.*, 2011) is subsumed here as the 'canonical' EC 1 macro-model, and its detailed derivation, updated in the context of this framework, can be found in Appendix A of the Supplementary Materials. Briefly, the derivation uses a combination of temporal separation of the three general processes [(rapid) reactant binding $>$ (intermediate) boundary electron transfer $\gg$ (rate-limiting) central electron transfer] and non-equilibrium thermodynamic force-to-flux relationship to unify the elementary reactions into a steady-state velocity equation with five kinetic parameters. This temporal separation is justifiable for most EC 1 enzymes. Because the central catalytic domain typically represents multiple sequential redox centers spread across most of the space within the enzyme (Fig. 1) and the rate of electron tunneling is inversely proportional to the distance between the redox centers (Ransac *et al.*, 2010), one can assume that electron tunneling over shorter distances at the periphery [Equations (5) and (7)] is fast compared with the electron tunneling over the large distance in the central catalytic domain [Equation (6)]. In addition, at physiological levels, e-carrier concentrations are typically at much higher levels than the EC 1 enzyme concentration, which allows one to assume rapid-equilibrium exchange between the free e-carrier species and the bound e-carriers of the EC 1 enzyme complex [Equations (1–4) and Fig. 1]. Alternative macro-models can be derived from the subtle differences in the assumptions applied, such as changing the kinetic mechanism for the formation of the catalytic enzyme–substrate complexes (see Appendix A of Supplementary Materials).

2.4 Bridging macro and micro-models: unitary rate constants

Because the micro-model is based on the same set of seven elementary reactions [Equations (1–7)] as the corresponding macro-model, the unitary rate constants governing the state transitions have direct relationships to the experimentally measurable steady-state kinetic parameters of the macro-model (Appendix D of Supplementary Materials). Thus, even though the micro-model has a much larger degree of freedom than the macro-model (138 versus 5), once the kinetic parameters and the thermodynamics of the reaction are known, one can narrow the parameter space of the micro-model significantly using the resulting constraints on the unitary rate constants. For the binding reaction groups (D1, D2, A1, A2) in Table 2, the unitary rate constants are related to the corresponding K_S saturation kinetic parameters according to the following equations:

$$K_{S,D} = \frac{kr_{D1}}{kf_{D1}}, K_{S,A} = \frac{kr_{A1}}{kf_{A1}} \tag{8}$$

$$K_{S,AD} = \frac{kr_{D2}}{kf_{D2}}, K_{S,DA} = \frac{kr_{A2}}{kf_{A2}} \tag{9}$$

For the boundary electron transfer reaction groups (BD, BA, TD, TA) assuming no difference between electron tunneling in the bimolecular and trimolecular states, the unitary rate constants are related to the corresponding K_R redox potential kinetic parameters according to the following equations:

$$K_{R,D} = \frac{kr_{BD}}{kf_{BD}} = \frac{kr_{TD}}{kf_{TD}} \tag{10}$$

$$K_{R,A} = \frac{kr_{BA}}{kf_{BA}} = \frac{kr_{TA}}{kf_{TA}} \tag{11}$$

For the catalytic reaction groups (UT, BT, TT), the unitary rate constants are related to the K_{eq} equilibrium constant and forward and reverse V_{max} maximum velocity kinetic parameters according to the following equation:

$$K_{eq} = \frac{V_{maxf}}{V_{maxr}} = \frac{kf_{UT}}{kr_{UT}} = \frac{kf_{BT}}{kr_{BT}} = \frac{kf_{TT}}{kr_{TT}} \tag{12}$$

While the catalytic unitary rates are calculated exactly from the parameter values and the thermodynamics of the reaction, estimates of the order of magnitude of the boundary electron transfer and binding rates are required (see Appendix D of Supplementary Materials).

2.5 Experimental data

To validate the models, kinetic experiments were carried out using a SAFAS UV mc2 spectrophotometer to measure the absorption of specific wavelengths of the substrate and/or product of the oxidation/reduction reaction catalyzed by the oxidoreductase of interest. The data and the experimental protocol are described in more details in our previous work (Chang *et al.*, 2011). Here we use four time series of substrate depletion corresponding to the initial concentrations of 25 μM, 50 μM, 75 μM and 100 μM of NADH and 5 μM of rat muscle mitochondria complex I. In the comparison with the simulated time series, both the substrate and enzyme concentrations in the time series are scaled up by a factor of 10 to represent typical *in vivo* concentration levels.

2.6 Simulation

The main prediction output of either the micro or macro-model is the time trajectory of the state variables from the solution of the ODEs. For macro-models, a differential equation is defined for each reactant concentration state variable based on the velocity equation of the reaction scaled by the stoichiometry of the reactant. For micro-models, a differential equation is defined for each of the 36 enzyme microstates, with each microstate represented as the number of enzyme molecules present in that state, each equation written as the balance between the incoming and outgoing transitions to the microstate and each transition defined by its unitary rate constant multiplied by the microstate(s) it originated from. Whereas ODEs based on velocity equation are simple to formulate, the complex arrangement of transitions for micro-models could benefit from a systematic computational approach. The RedoxMech software addresses this challenge.

2.6.1 RedoxMech RedoxMech is a computational tool that allows one to easily implement, simulate and analyze the various EC 1 micro-models generated through the framework presented in this article. It is a

language extension and an add-on to xCellerator (Shapiro *et al.*, 2003), which allows it to leverage xCellerator's simple reaction arrow notations to programmatically generate various types of reaction mechanisms such as mass action kinetics for elementary catalytic and non-catalytic reactions and various regulatory relationships, along with catalytic reaction mechanisms involving multiple substrates and products through kMech (Yang *et al.*, 2005), an earlier language extension of xCellerator. Reactions created through RedoxMech, kMech and xCellerator notations can all be interpreted simultaneously by xCellerator into a system of ODEs for deterministic simulation via an ODE solver such as NDSolve, or an array of stochastic transition functions for stochastic simulations via Gillespie's SSA, which is an 'exact' stochastic method that exhaustively simulate every reaction process based on their probability of occurrence (Gillespie, 1977). In addition, xCellerator has the built-in capability to export the ODEs generated in Mathematica to the widely used SBML standard for better sharing among the modeling community.

As an xCellerator language extension, RedoxMech provides a new modular arrow input notation for generating the intra-enzyme reaction network of an EC 1 enzyme:

$$\mathrm{EC1}\left[\{\mathrm{Dre},\mathrm{Dox}\} \overset{\mathrm{Enz}}{\rightleftarrows} \{\mathrm{Are},\mathrm{Aox}\}, \mathrm{SSConst}, \mathit{Options}\right] \tag{13}$$

where Dre, Dox, Are, Aox, and Enz are variables one can use to specify the name of the donor e-carrier species, acceptor e-carrier species and enzyme, respectively. SSConst is entered as a list of known steady-state kinetic parameters obtained for the complex (can be a blank list {}), which is automatically converted to the appropriate unitary rate constants in the intra-enzyme reaction network based on the estimation rules described earlier. *Options* consists of four optional switches: *ReactionType*, *ManualList*, *RemoveList* and *Output*. By default, the EC 1 arrow notation generates a micro-model based on the complete intra-enzyme reaction network. However, the user may either specify a pre-encoded (sub)set of reactions (e.g. '*Ping-Pong*', '*Ordered*', '*Random*') through the *ReactionType* option, or manually defining a list of transition pairs through the *ManualList* option. *RemoveList* allows the user to specifically remove any of the 69 built-in internal network transition pairs. *Output* switches the output from the default '*xCellerator*' reaction list to pass through to xCellerator for interpretation and simulation, or a '*Matrix*' format that can be passed alternatively to the support function **ReactionMatrix** to produce a more visually informative mapping of the intra-enzyme reaction network in terms of a matrix of state transitions. In addition, an automatic King–Altman method that was originally implemented in Mathematica by Mulquiney and Kuchel (2003) has been extended in RedoxMech as the function **SSVelocityEq**, which derives steady-state velocity equations for specific EC 1 mechanisms directly from the reaction matrix that the EC 1 arrow notation produces (see example in Appendix C and Mathematica notebook in the Supplementary Materials).

3 RESULTS AND DISCUSSION

3.1 Synergistic uses of micro and macro-models

3.1.1 Pre–steady-state kinetics To verify that the two models can reproduce the experimental results, we show how a set of concentration time–series outputs from both the complete micro-model (all 69 transition pairs) and the general macro-model (derived in Appendix A of Supplementary Materials) compare with the *in vitro* enzyme kinetics data on the complex I of rat muscle mitochondria homogenate obtained from our previous work (Chang *et al.*, 2011). The steady-state parameters of the macro-model are fitted to the various experimental data time series of different initial substrate concentration [NADH]. Then, they are used to constrain the unitary rate constants of the micro-model based on the estimation rules described earlier (a complete list of parameter values can be found in Appendix D of Supplementary Materials). The resulting concentration time–series comparisons in Figure 2A not only show consistent agreement between the two models and the experimental data, but also show how the outputs of the two modeling approaches differ in a predictable way. In particular, the outputs of the micro-model are consistently ahead of the corresponding outputs of the macro-model in the initial period. This is due to the macro-model's assumption of steady-state condition from the start, whereas the micro-model explicitly models the elementary reactions so that its output accounts first for the pre–steady-state transient period in which there is a rapid quenching of substrate concentration when the substrate molecules first bind with the ensemble of enzymes. Another way of comparing the two models is through the simulated flux time series of the enzyme reaction that are calculated from the derivative of the reactant concentrations. Figure 2B again shows general agreement in the curvatures of the flux time series except for the small offset at the start and end of the reaction due to the pre–steady-state kinetics. However, whereas all reactants in the macro-model have the same flux time

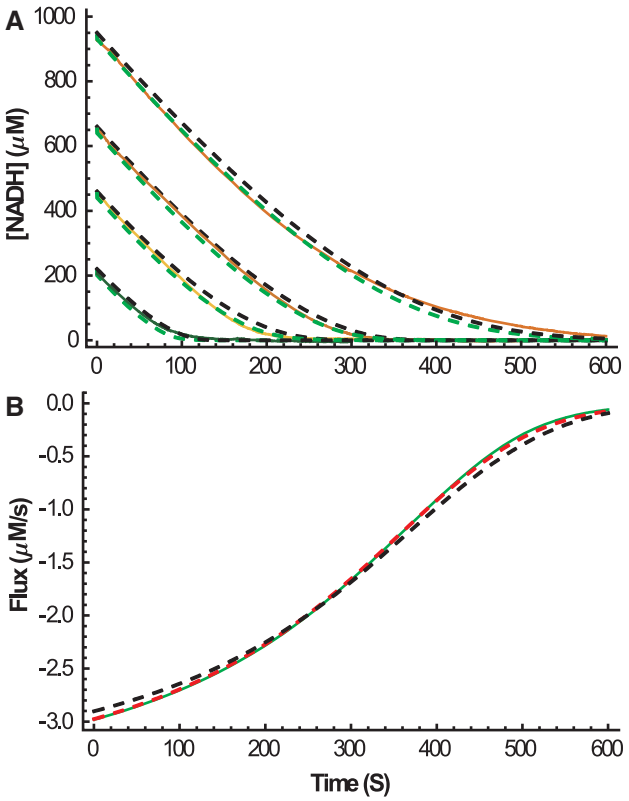

Fig. 2. Comparing micro and macro Models. (**A**) Simulated concentration time-series versus experimental data. Black dashed lines represent macro-model output, green dashed lines represent the micro-model output, and all others are experimental data curves with varying initial concentration. (**B**) Simulated flux time series. Black dashed lines represent macro-model flux, green solid line represents the rate of change of D^{red} of the micro-model, and the dashed red line represents rate of change of A^{ox} of the micro-model

series, in the micro-model, the fluxes of the reactants are not necessarily the same, as shown by the slight difference in the derivative of the D^{red} concentration and A^{ox} concentration in Figure 2B. This effect is a direct result of differences in the binding/unbinding sequence of the reactants in the micro-model, which is shown even more clearly in the flux time series of different EC 1 mechanisms in Figure 7B.

3.1.2 Stochastic fluctuations A deterministic reaction model can provide an accurate description when the stochastic fluctuations are negligible, which is typically the case with large number of molecules in solution. Although this may be the case with *in vitro* conditions, *in vivo* conditions within a cell or a cell's organelle may have significantly lower volume and fewer molecules so that stochastic fluctuations may become important. Figure 3 shows the distribution of 25 individual simulations of the complete micro-model under a reaction volume of $1\,\mu m^3$, roughly the volume of one mitochondrion. The stochastic concentration time series are then used to find the mean, 1-SD-away and 2-SD-away time trajectories to summarize the variance of the reaction as shown in the overlay of the individual trajectories. Figure 3 also shows how consistently the average of the stochastic time–series trajectories from SSA simulation of the micro-model overlaps and follows the time series predicted by deterministic ODE simulation of the micro-model. We note that, although the exactness of the SSA produces accurate statistical results, it is computationally expensive and can become intractable as the reaction system size grows. Nevertheless, it is useful in simulating smaller reaction systems and obtaining characteristic variations for that system.

3.2 Encoding specific mechanisms of EC 1

As mentioned earlier, by selectively encoding the set of transition pairs in the micro-model, the resulting intra-enzyme reaction network can represent specific kinetic mechanisms of EC 1. Here we present how the micro-model can generate and extend the commonly used Bi Bi ternary enzyme mechanisms based on the concise rules and nomenclature introduced by Cleland such as the Ping-Pong, the Ordered Sequential and the Random Sequential mechanisms (Cleland, 1963). Additionally, we note that many other variations of the Bi Bi mechanisms can also be obtained from the common ones by applying relative values of the unitary rate constants to emulate special limiting cases, e.g. the Theorell–Chance mechanism as the special case of Ordered Sequential mechanism.

3.2.1 Ping-Pong mechanism The classical Ping-Pong mechanism partitions the overall ternary enzyme reaction into (i) an ordered sequence of binding and releasing of the first substrate and product, which leaves a modified form of the enzyme En^-, and (ii) a second ordered sequence of binding and releasing of the second substrate and product, which restores the original enzyme form En. Figure 4A shows that when the Ping-Pong mechanism is applied to a typical oxidoreductase reaction, it partitions the catalysis of the reaction into two distinct steps, $D^{red}En \Leftrightarrow D^{ox}En^-$ and $En^-A^{ox} \Leftrightarrow EnA^{red}$, instead of just one central catalytic event. In the context of the micro-model, the separation of the catalytic event means that a Ping-Pong EC 1 complex only operates within the bimolecular states. Furthermore, the specific order of binding and releasing ensures that there is only a unique occurrence of the seven basic transition events. However, with the introduction of two intra-enzyme reaction centers R_H and R_L, there are now two possible sequence variations for when the modified enzyme form En^- binds with the acceptor e-carrier because En^- can undergo internal electron transfer either before or after complexing with the second substrate. From the 69 transition pairs, a Ping-Pong EC 1 complex can be encoded using the reaction group listed in Table 2 as shown in Figures 4B and C. The index number for each reaction group specifies a particular reaction within the reaction group (see also Appendix B of Supplementary Materials).

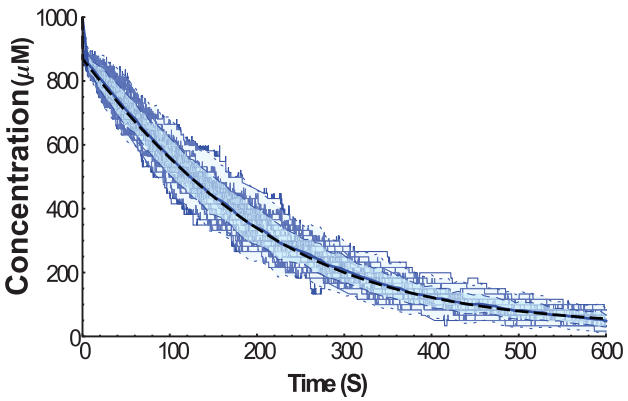

Fig. 3. Stochastic simulations and variances. Twenty-five SSA time series overlayed with the mean (central blue line), 1 SD away from the mean (dashed lines enclosing the blue shaded region), 2 SDs away from the mean (dotted lines enclosing the region) and the output of the deterministic simulation (central black dashed line)

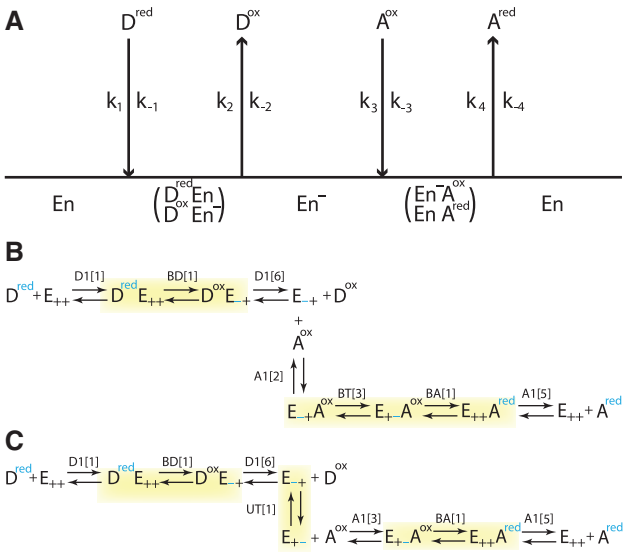

Fig. 4. Ping-Pong Bi Bi reaction. (**A**) Classical mechanism sequence. (**B**) EC 1 intra-enzyme reaction network encoding number 1. (**C**) EC 1 intra-enzyme reaction network encoding number 2. Highlighted sections represent electron transfer reactions, and symbols 'red' and '−' indicate electron positions

3.2.2 Ordered Sequential mechanism The classical Ordered Sequential mechanism prescribes a specific order of substrate-binding events to form the central ternary complex for catalysis, which is followed by a specific order of product-releasing events. Note that because there are two substrates and two products, there are four permutations of how the sequence order of binding/unbinding could proceed. One example of the sequence order, when applied to the oxidoreductase reaction, consists of the binding of reduced species of donor e-carrier D^{red}, the binding of oxidized species of acceptor e-carrier A^{ox}, the catalytic transfer of electron in the ternary complex, the release of oxidized species of donor e-carrier D^{ox} and finally the release of reduced species of acceptor e-carrier A^{red} (Fig. 5A). As in the case of the Ping-Pong mechanism, the Ordered Sequential mechanism can be encoded by the minimum number of transitions, as shown in Figure 5B. In contrast, however, all the electron transfer steps operate in the trimolecular states. With the addition of the boundary electron transfer reactions introduced in the framework, the catalytic part of the reaction is expanded according to a linear sequence of Equations (5–7). To emulate the Theorell–Chance mechanism, a special case of Ordered Sequential mechanism where the steady-state level of the trimolecular states are very low, the unitary rate constants for the reactions leading to the bimolecular complexes need to be set very large compared with the unitary rate constants leading to the trimolecular complex or the unimolecular enzyme (Leskovac, 2003).

3.2.3 Random Sequential mechanism In the classical Random Sequential mechanism, the sequence order of the substrates binding and products unbinding is random, which effectively encompasses all four permutations of the Ordered Sequential mechanism simultaneously. At any time, either one of the substrates can bind first, while either product can unbind first from the complex (Fig. 6A). Similar to the Ordered Sequential mechanism, the catalysis of the reaction is expanded according to a linear sequence of Equations (5–7), but its encoding is expanded to 11 elementary reaction pairs to incorporate all sequence permutations (Fig. 6B). RedoxMech has all three Bi Bi mechanisms pre-encoded so that one only needs to specify the option (e.g. *ReactionType* → '*Random*') in the EC 1 arrow notation shown in Equation (13). A convenient function for inspecting the intra-enzyme reaction network visually is **ReactionMatrix**, which displays a matrix composed of a list of initial microstates as rows and a list of final microstates as columns such that each matrix entry represents the transition rate between the microstates. An example is shown for the Random mechanism of an EC 1 complex in Table 3.

3.2.4 Comparing the effects of specific mechanisms Besides the steady-state parameters, the time–series output of a micro-model is also directly affected by the specific mechanism encoded in its intra-enzyme reaction network. Figure 7 shows how models of the various Bi Bi mechanisms described earlier (Ping-Pong, Ordered Sequential and Random Sequential) compare with the complete model using the full intra-enzyme reaction network in both their concentration time series of free D^{red} (not bound to the enzyme) and flux time series of substrate e-carrier species (D^{red} and A^{ox}). All four models share the same steady-state parameter values. The pre–steady-state period of the concentration time series shows both the time it takes for the reaction system to reach steady-state saturation, as indicated by duration of the initial drop (offset) in concentration due to the binding of the reactant with the complex, and the total offset amount when reaching steady state (Fig. 7A). The biggest difference is in the offset of the free D^{red} concentration of the complete model, which doubles in magnitude (twice that of enzyme concentration) compared with the other models. This is likely due to the complete model using all bimolecular and trimolecular states, and the

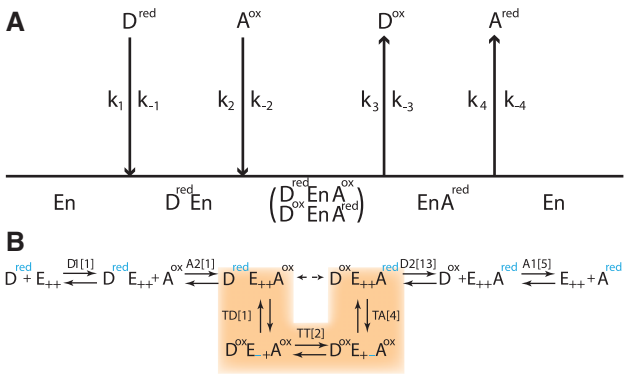

Fig. 5. Ordered Sequential Bi Bi reaction. (**A**) Classical mechanism sequence. (**B**) EC 1 intra-enzyme reaction network encodings. Highlighted sections represent electron transfer reactions, and symbols 'red' and '–' indicate electron positions

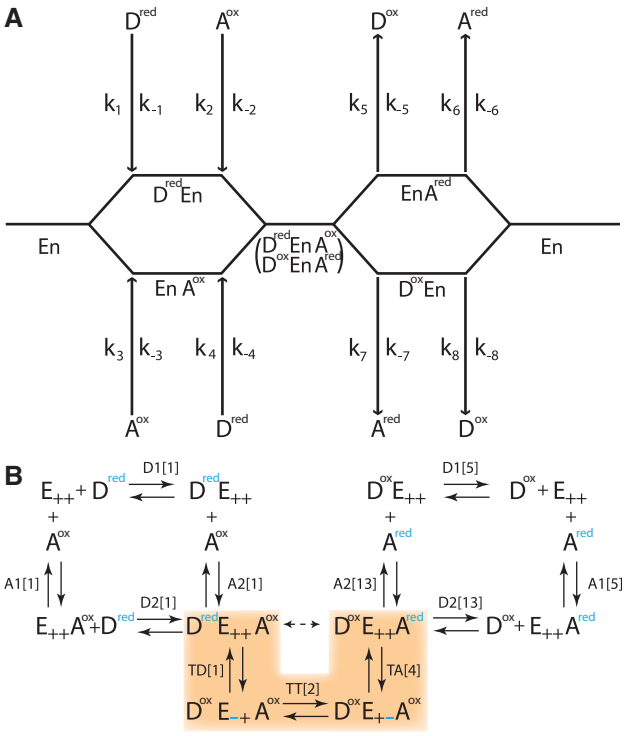

Fig. 6. Random Sequential Bi Bi Reaction. (**A**) Classical mechanism sequence. (**B**) EC 1 intra-enzyme reaction network encodings. Highlighted sections represent electron transfer reactions, and symbols 'red' and '–' indicate electron positions

Table 3. Random sequential EC 1 reaction matrix

	Epp	Dox ◇ Epp	Dre ◇ Epp	Epp ◇ Aox	Epp ◇ Are	Dox ◇ Enp ◇ Aox	Dox ◇ Epn ◇ Aox	Dox ◇ Epp ◇ Are	Dre ◇ Epp ◇ Aox
Epp	0	Dox kf_{D1}[5]	Dre kf_{D1}[1]	Aox kf_{A1}[1]	Are kf_{A1}[5]	0	0	0	0
Dox ◇ Epp	kr_{D1}[5]	0	0	0	0	0	0	Are kf_{A2}[13]	0
Dre ◇ Epp	kr_{D1}[1]	0	0	0	0	0	0	0	Aox kf_{A2}[1]
Epp ◇ Aox	kr_{A1}[1]	0	0	0	0	0	0	0	Dre kf_{D2}[1]
Epp ◇ Are	kr_{A1}[5]	0	0	0	0	0	0	Dox kf_{D2}[13]	0
Dox ◇ Enp ◇ Aox	0	0	0	0	0	0	kf_{TT}[2]	0	kr_{TD}[1]
Dox ◇ Epn ◇ Aox	0	0	0	0	0	kr_{TT}[2]	0	kf_{TA}[4]	0
Dox ◇ Epp ◇ Are	0	kr_{A2}[13]	0	0	kr_{D2}[13]	0	kr_{TA}[4]	0	0
Dre ◇ Epp ◇ Aox	0	0	kr_{A2}[1]	kr_{D2}[1]	0	kf_{TD}[1]	0	0	0

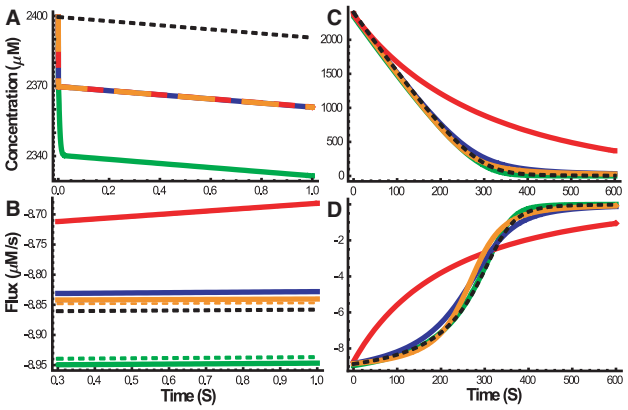

Fig. 7. Comparison of concentration and flux time series. (**A**) D^{red} concentration at 1 s. (**B**) EC 1 flux at 1 s. (**C**) D^{red} concentration at 10 min. (**D**) EC 1 flux at 10 min. Black dashed lines = macro-model, green lines = EC 1 complete mechanism, blue lines = EC 1 Ordered mechanism, orange lines = EC 1 Random mechanism, red lines = EC 1 Ping-Pong mechanism. For (B) and (D), solid color series represent rate of change of D^{red}, whereas the dashed color series represent rate of change of A^{ox}

extra states absorb more of free D^{red} in comparison with the other submechanisms. The differences in the free concentration offset across the four reactants can also reveal their relative position in the order of the reaction. The corresponding pre–steady-state flux comparison in Figure 7B shows that the flux of the Ping-Pong model is already decelerating, whereas others are still maintaining a constant value. In addition, the difference in the flux of the substrate species is markedly smaller in the Ping-Pong model. Both effects are likely to be caused by disruptions to the electron transfer sequence by the binding reactions, which favor the reverse transitions in the intra-enzyme reaction network. From the complete time series in Figures 7C and D, it can been seen that the bimolecular mechanism of the Ping-Pong model produces a distinctively slower conversion of substrates than the trimolecular mechanisms in the other models. Predictably, the complete model is the fastest, followed by the Random model, Ordered model and finally the Ping-Pong model, in the order of decreasing number of possible electron traveling paths.

3.3 Cascading EC 1 pathway or supercomplex

Some of the most prominent oxidoreductases are organized physiologically inside membranes to perform cascades of electron transfer reactions (Mitchell, 1969; Nicholls and Ferguson, 2002). These EC 1 complexes can either rely on the intermediate e-carriers that freely diffuse in the plane of the membrane to chain the complexes together in a linear pathway, or alternatively, the complexes can form aggregates or supercomplexes to enable direct electron channeling (Boekema and Braun, 2007). Through its modular approach, RedoxMech enables one to programmatically define and simulate cascading EC 1 reactions in either a pathway or supercomplex setting, with the ability to define the conditions in which the dynamics may switch (see Supplementary Mathematica notebook).

4 CONCLUSION

We have introduced a general microscopic framework for the kinetic modeling of Bi Bi oxidoreductases by decomposing their redox capabilities into seven elementary reactions. By using different combinations of enzyme state transitions, this approach enables and subsumes more specialized models for specific members of the family, or specific conditions. Furthermore, in the steady-state regime, the approach leads to macroscopic rate equations consistent with previous derivations and with experimental data, unifying both microscopic and macroscopic approaches for modeling enzymatic reaction of EC 1. Because the microscopic models are composable, the generality of the approach can also be used to model EC 1 supercomplexes as cascades of individual complexes. In addition, the microscopic framework allows incorporation of elementary binding reactions of specific inhibitory reactants to enable modeling of regulatory control mechanisms, as well as alternative electron transfer reactions to enable modeling of slippage mechanisms involved in reactive oxygen species production. Altogether, this framework provides a way to flexibly and programmatically describe the core enzymes of cellular energetics for possible integration into future comprehensive models of metabolism that will further our understanding of the central role bioenergetics play, not only in the maintenance of life but also in disease and aging.

Funding: National Institute Health (grants LM010235-01A1 and 5T15LM007743) (in part), and NSF (grant 0513376 to P.B.).

Conflict of Interest: none declared.

REFERENCES

Benard,G. *et al.* (2006) Physiological diversity of mitochondrial oxidative phosphorylation. *Am. J. Physiol. Cell Physiol.*, **291**, C1172.

Berry,S. (2002) The chemical basis of membrane bioenergetics. *J. Mol. Evol.*, **54**, 595–613.

Boekema,E. and Braun,H. (2007) Supramolecular structure of the mitochondrial oxidative phosphorylation system. *J. Biol. Chem.*, **282**, 1.

Brandt,U. (2006) Energy converting NADH: quinone oxidoreductase (complex i). *Annu. Rev. Biochem.*, **75**, 6992.

Chang,I. *et al.* (2011) Modeling of mitochondria bioenergetics using a composable chemiosmotic energy transduction rate law: theory and experimental validation. *PloS ONE*, **6**, e14820.

Chen,X. *et al.* (2010) Kinetics and regulation of mammalian NADH-ubiquinone oxidoreductase (Complex i). *Biophys. J.*, **99**, 1426–1436.

Cleland,W. (1963) The kinetics of enzyme-catalyzed reactions with two or more substrates or products: I. Nomenclature and rate equations. *Biochim. Biophys. Acta*, **67**, 104–137.

Cornish-Bowden,A. (1977) An automatic method for deriving steady-state rate equations. *Biochem. J.*, **165**, 55.

Gillespie,D.T. (1977) Exact stochastic simulation of coupled chemical reactions. *J. Phys. Chem.*, **81**, 2340–2361.

Klepeis,J. *et al.* (2009) Long-timescale molecular dynamics simulations of protein structure and function. *Curr. Opin. Struct. Biol.*, **19**, 120–127.

Leskovac,V. (2003) *Comprehensive Enzyme Kinetics*. Kluwer Academic/Plenum Publishers, New York, pp. 10013–1578.

Mitchell,P. (1969) Chemiosmotic coupling and energy transduction. *Theor. Exp. Biophys.*, **2**, 159–216.

Mulquiney,P.J. and Kuchel,P.W. (2003) *Modelling Metabolism with Mathematica*. CRC Press, Boca Raton, FL.

Nicholls,D.G. and Ferguson,S.J. (2002) *Bioenergetics 3*. Academic Press, London.

Ransac,S. *et al.* (2008) The loneliness of the electrons in the bc1 complex. *Biochim. Biophys. Acta*, **1777**, 1053–1059.

Ransac,S. *et al.* (2010) The fitting of electrons in complex i: a stochastic approach. *Biochim. Biophys. Acta*, **1797**, 641–648.

Rao,C. and Arkin,A. (2003) Stochastic chemical kinetics and the quasi-steady-state assumption: application to the gillespie algorithm. *J. Chem. Phys.*, **118**, 4999.

Selivanov,V.A. *et al.* (2009) Bistability of mitochondrial respiration underlies paradoxical reactive oxygen species generation induced by anoxia. *PLoS Comput. Biol.*, **5**, e1000619.

Selivanov,V.A. *et al.* (2011) Reactive oxygen species production by forward and reverse electron fluxes in the mitochondrial respiratory chain. *PLoS Comput. Biol.*, **7**, e1001115.

Shapiro,B. *et al.* (2003) Cellerator: extending a computer algebra system to include biochemical arrows for signal transduction simulations. *Bioinformatics*, **19**, 677–678.

Sin,G. *et al.* (2009) Application of modeling and simulation tools for the evaluation of biocatalytic processes: a future perspective. *Biotechnol. Prog.*, **25**, 1529–1538.

Vinogradov,A. (2008) NADH/NAD+ interaction with NADH: ubiquinone oxidoreductase (complex I). *Biochim. Biophys. Acta*, **1777**, 729–734.

Yang,C. *et al.* (2005) An enzyme mechanism language for the mathematical modeling of metabolic pathways. *Bioinformatics*, **21**, 774–780.